Mechanics of Materials 148 (2020) 103522

Contents lists available at ScienceDirect

Mechanics of Materials

journal homepage: www.elsevier.com/locate/mechmat

Research paper

A machine learning based approach for determining the stress-strain relation of grey cast iron from nanoindentation

Jian Weng[a,b], Rebecka Lindvall[b], Kejia Zhuang[a,*], Jan-Eric Ståhl[b], Han Ding[a,c], Jinming Zhou[b]

[a] Hubei Digital Manufacturing Key Laboratory, School of Mechanical and Electronic Engineering, Wuhan University of Technology, Wuhan 430070, China
[b] Division of Production and Materials Engineering, Lund University, Lund 22100, Sweden
[c] State Key Laboratory of Digital Manufacturing Equipment and Technology, Huazhong University of Science and Technology, Wuhan 430074, China

ARTICLE INFO

Keywords:
Nanoindentation
Stress-strain relation
Machine learning
Inverse calculation

ABSTRACT

Apart from microhardness and elastic modulus, the stress-strain relation is another important characteristic that more and more scholars have been trying to extract from nanoindentation. With the development of artificial intelligence and computer technology, a machine learning based method is proposed in this paper to extract stress-strain curve of grey cast iron using sharp nanoindentation. Firstly, the average curve is achieved by the grid-design nanoindentation to avoid the influence of different phases on indentation results. The plastic behavior is considered as a power law function in this paper. Then, finite element method supports to generate a simulation data set, with full-factor and full-level design of constants of stress-strain relation. With the simulation data set, the support vector regression machine establishes a surrogate model to correlate the input (constants of stress-strain function) and output (the mean error between predicted and measured results). The best parameters of support vector machine are determined through grid search and cross-validation. PSO serves as the optimization algorithm to find the optimum of input related to the measured results, with an inertia factor to improve the local search ability. Finally, the simulation loading curve with the optimal constants provided by PSO perfectly fits the measured loading curve, which shows the effectiveness of the inverse method proposed in this paper.

1. Introduction

Nanoindentation is an important method that can evaluate the micromechanical properties of materials with a small piece of sample, which makes it more advanced than the conventional tension or compression tests (Golovin, 2008). The measurement is within nanoscale or microscale, allowing the identification of local characteristics of different phases, composites or microstructures. Usually, nanoindentation is applied to calculate the hardness and elastic modulus of materials based on the loading and unloading curves (Fischer-Cripps, 2006). During the past decades, more and more researches are proposed to extend the application of nanoindentation, for instance, the measurements of residual stress and stress-strain relation (Dean et al., 2011; Long et al., 2017; Ma et al., 2012b; Patel and Kalidindi, 2016).

When it comes to the determination of stress-strain relation using instrumented indentation, there are three kinds of approaches mainly used, analytical methods, empirical methods, and FEM (Finite Element Method) supported methods. Analytical methods always require a spherical indenter due to the consideration of the convergence of the calculated results (Pathak and Kalidindi, 2015). The analytical concept of indentation stress-strain relation is first introduced by Tabor (2000), presenting that the stress can be defined as the mean pressure in contact area while the strain can be defined as 0.2 of the ratio of contact radius to indenter radius. The definition of indentation strain is now more commonly chosen as the ratio of contact radius to effective indenter radius, which is proved more powerful to capture the elastic and plastic material response (Kalidindi and Pathak, 2008). Donohue et al. (2012) discussed the difference when using different definitions of contact radius and indentation strain, the results show significant influence of definitions on stress-strain curves. The analytical methods always obtain one point on stress-strain curve using a loading and unloading test, which means a large number of instrument tests are required to achieve full stress-strain curve (Pathak et al., 2009). Moreover, with the development of nanoindentation systems, CSM (Continuous Stiffness Measurement) is sometimes used to enhance the calculation of stress-strain relation (Weaver and Kalidindi, 2016).

Empirical models represent a large number of researches that try to find a simplified numerical expression of variables in Nanoindentation. Collin et al. (2008) proposed a polynomial function to describe the relationship between mechanical properties and detailed geometric

* Corresponding author: Kejia Zhuang

https://doi.org/10.1016/j.mechmat.2020.103522
Received 2 January 2020; Received in revised form 25 April 2020; Accepted 24 June 2020
Available online 25 June 2020

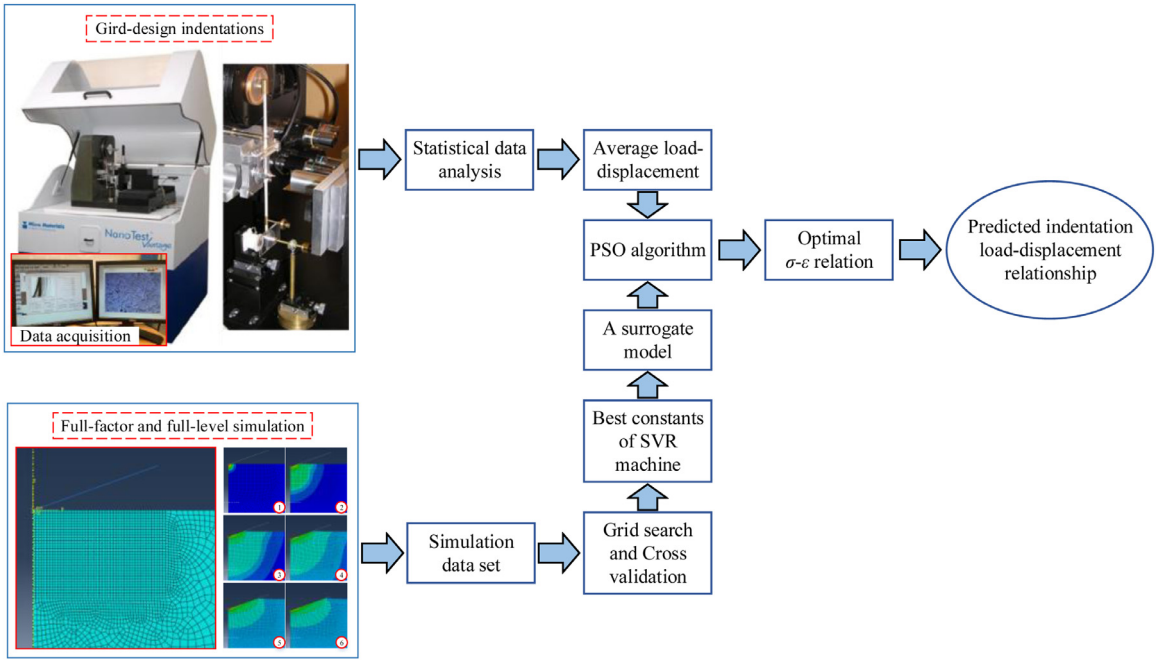

Fig. 1. The procedure of the method proposed in this paper.

information in spherical indentation. Kucharski and Mróz (2007) also proposed a complex model describing the load curve based on materials properties, which assumes that the load curve is a weighted average of hardening behavior and perfect plastic deformation. For the sharp indenter, several attempts are also done to establish a correlation among the characteristics. Giannakopoulos (Giannakopoulos and Suresh, 1999) pointed out that the stress corresponding to 0.29 strain is a crucial value to determine the load curve and presented a load curve function for very ductile material. The dimensionless analysis is also an important part of empirical modeling, which attempts to find a constant or regular-change value among the characteristics given by Nanoindentation (Zhang et al., 2018). A set of dimensionless functions are given by Dao et al. (2001) to characterize the sharp indentation curves, applying a wide range of mechanical properties. These dimensionless functions can help to establish the inverse method for the determination of elastic-plastic behavior from indentation curves.

FEM supported methods that depend on the computation of finite element analysis are designed to achieve the stress-strain relation by minimizing the errors between predicted and measured results. The advantages of this kind of methods are obvious, for instance, independent of the definitions of strain and stress, perfect stress-strain relation without noise, independent of multiple tests (only one indentation curve is enough). A so-called 'SSCUBONI' (Stress Strain CUrve Based On Nanoindentation) is first proposed by Bouzakis et al. (2001), adopting a step-by-step finite element analysis to calibrate the stress-strain curve. This approach can provide a segmentation curve to describe the elastic-plastic behavior of thin hard coating, depending on the manual adjustments of input parameters. Moy et al. (2011) proposed an inverse method integrated with a batch deterministic approach and optimization algorithm to calculate the elastic modulus, yield stress, and strain hardening factor. This method starts with an initial couple of parameters and adjusts them after each simulation based on the gradient of objective with respect to the variation of parameters. Hamim and Singh (2017) presented a surrogate model-based method to correlate the parameters of stress-strain curve and loading curve, considering a simplified linear plastic response. A set of simulation data is first generated by Taguchi design in his method. Then, a method integrated with principal component analysis and Radial Basis Functions is used to establish a model to replace the Finite element simulations. His-research did not cover the content of finding the optimal stress-strain parameters to minimize the errors between predicted and measured results.

As stated above, many scholars attempted to extract the elastic-plastic behavior, i.e. stress-strain relation from instrumented nanoindentation through different methods and theories. However, there is still a need for a more intelligent and effective method to solve this problem. In this paper, an inverse method integrated with machine learning tool and meta-heuristic algorithm is proposed to achieve the stress-strain curve of grey cast iron supported by finite element computation. The mapping of hardness, modulus and creep distance is obtained by grid-design nanoindentation. The statistical results of the variation of load with respect to indentation depth are obtained to show the macro response of grey cast iron. An accurate finite element model is established in ABAQUS using an axisymmetric model to replace the sharp indentation with Berkovich indenter to save the computation time. A power law plastic behavior is considered as the constitutive material model to describe the stress-strain relation, with three constants need to be calibrated. SVR (Support Vector Regression) serves to propose a surrogate model using the data set provided by full-factor and full level finite element simulations. The optimal parameters of support vector machine is calculated by cross-validation and grid search supported by the machine learning tool LIBSVM. Finally, PSO (Particle Swarm Optimization) serves to search the optimum of constants in stress-strain relation that can provide a simulation result perfectly fit the measured results. The optimum of the constants is entered into the finite element model to validate the correctness of the method proposed in this paper.

2. Overview of the methodology

The procedure of the inverse method to calibrate the stress-strain relation of grey cast iron from nanoindentation based on machine learning, finite element simulation, and optimization algorithm is illustrated in Fig. 1. The first step is to perform a grid-design indentation tests using instrumented nanoindentation. Then, generate the simulation data set supported by ABAQUS. The establishment of a surrogate model that can calculate instead of FEM is done by the machine learning tool LIBSVM. PSO serves to quick search of the optimal stress-

strain relation considering the objective maximum load of experiments, which is done by MATLAB. Consequently, the optimal strain-stress relationship is entered into FEM to obtain the predicted load-displacement curve, which can be compared to the average curve to validate the effectiveness and correctness of the method proposed in this paper. The detailed information of the methodology are described in the following sections.

3. Nanoindentation of grey cast iron

3.1. Experimental setup

The material studied in this paper is grey cast iron which is widely used in the auto industry, especially for the brake disc and flywheel. The piece is cut out from a new casted brake disc. The sample preparation used is cold mounting to avid the thermal effect caused by hot mounting. The high temperature will result in aging of the material, which make difference to the measurement results.

Nanoindentation is now widely used in both academic and commercial organizations. Oliver and Pharr (2004) first introduced this method and used fuse silicon as a standard material for measuring mechanical properties by instrumented indentation. As mentioned above, this technique allows measurements of very small-scale mechanical behavior, which makes it sensitive to the consistency of materials. However, due to the actual industrial requirements, the macro performance achieves more attention from the manufacturers. Grid-design Nanoindentation is an important method to get a statistical result of the loading and unloading curve, capturing the material response given by different phases (Chen et al., 2015). In this section, a 15 × 15 matrix serves to obtain the average loading and unloading curve, utilizing a NanoTest Vantage4 nanoindentation system. The maximum load is fixed as 50mN while the load rate is 2.5mN/s. The dwell time at maximum load is 5 s. The surface topography of grey cast iron shown in microscope is given in Fig. 2(a). It can be seen that the material is inconsistent in microscale, so that the nanoindentation can be very sensitive to what kind of material is pressed during the loading period. The measured hardness can be very high if the indenter targets on the hard particles, while very low if the indenter targets on the graphite blocks. When the indenter targets on the graphite flakes, the material response will be affected by both bulk material and graphite, resulting in an irregular loading curve. Fig. 2(b) shows the raw data given by the grid-design nanoindentation, which illustrates a wide range of distribution. Thus, grid-design nanoindentation is necessary when investigating the mechanical properties of grey cast iron to achieve a statistical result.

Moreover, the description of grid-design nanoindentation are given in Fig. 3. As shown in Fig. 3(a), the microstructure of grey cast iron is inconsistent due to the irregular distribution of graphite in the bulk material. It can be easily found in Fig. 3(b) that the pits left by indenter are different. The pits are larger when the indenter hit graphite, which means the material is softer. Also, the graphite can be at the subsurface, which leads to an irregular load curve.

3.2. Discussions and statistical results

To our best knowledge, the measured properties can be affected by many factors, for instance, the maximum load, indentation rate, indentation depth. These effects achieve much attention when studying thin films or coatings (Ma et al., 2008, 2012a). However, in the experimental work of this paper, these factors are fixed for each indents to obtain a statistical results. The influence of different phases on the material response is the main focus in this section. Figs. 4(a) − 4(c) illustrate a brief view of the mapping of different mechanical properties, including hardness, elastic modulus and creep distance. Figs. 4(d) − 4(f) is the corresponding histograms.

It can be noted from Fig. 4 that the presence of flake graphite results in significant difference of the measured response, which shows the necessity of statistical analysis of the measured curves. The maximum hardness can be up to 6.6 GPa while the minimum can be down to 0.64 GPa. The variation of elastic modulus is more significant that ranges from 3 GPa to 218 GPa. When it comes to the creep distance, the range is from 0.7 nm to 26 nm. The dense distribution of the three measured properties is around 3.3 GPa, 170 GPa and 11 nm, respectively. The wide range of the distributions of these properties can be contributes to the significant difference between iron and graphite. The content of graphite results in extreme different material response, which emphasizes the importance of grid indentation and statistical analysis.

The macro behavior of grey cast iron is achieved by calculating an average curve from all the indentation results in this paper. Fig. 5 is the average result of all the loading and unloading curves given by grid-design nanoindentation. This curve is obtained by calculating the mean value of depth of all the indentations at the same load. It can be observed that the average curve shows a perfect trend of loading and unloading curve, which indicates the effectiveness of the grid-design nanoindentation on representing a macro behavior of bulk material.

4. Finite element modeling

4.1. Model settings

So far, FEM is the most effective and widely used method to model the procedure of nanoindentation. The simulation of nanoindentation can be simplified to a two-dimensional axisymmetric model for both spherical and Berkovich indenter, which has been validated by many scholars (Schwarm et al., 2017). In this section, ABAQUS serves for the simulations of nanoindentation with Berkovich indenter.

The Young's modulus is set as $E = 149$ GPa, which is obtained from the average value of all the nanoindentation using Oliver's method (Oliver and Pharr, 2004). This result is similar to the ordinary result given in other literature (155 GPa) (Ripley and Kirstein, 2006).

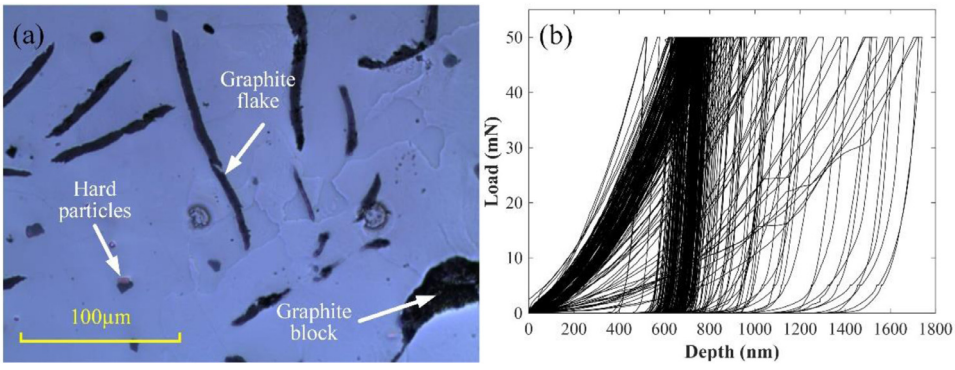

Fig. 2. (a) the surface topography of grey cast iron; (b) the distribution of loading and unloading curves given by grid-design nanoindentation.

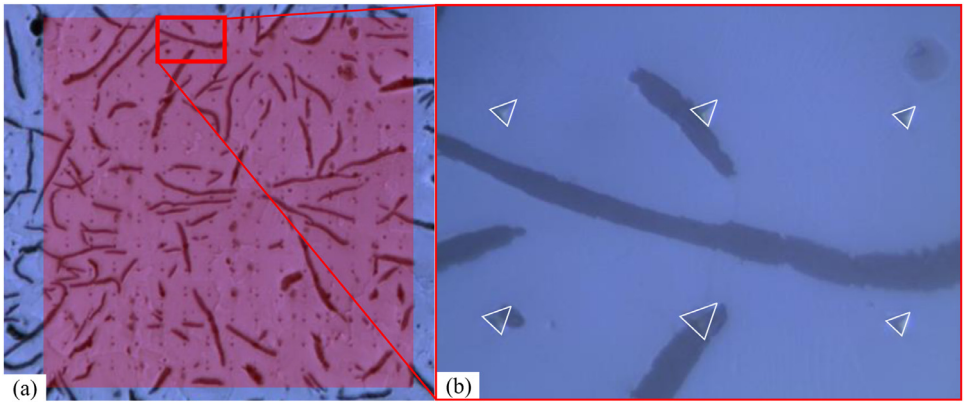

Fig. 3. The grid-design nanoindentation of grey cast iron; (a) general view of the matrix; (b) local view of the indentation.

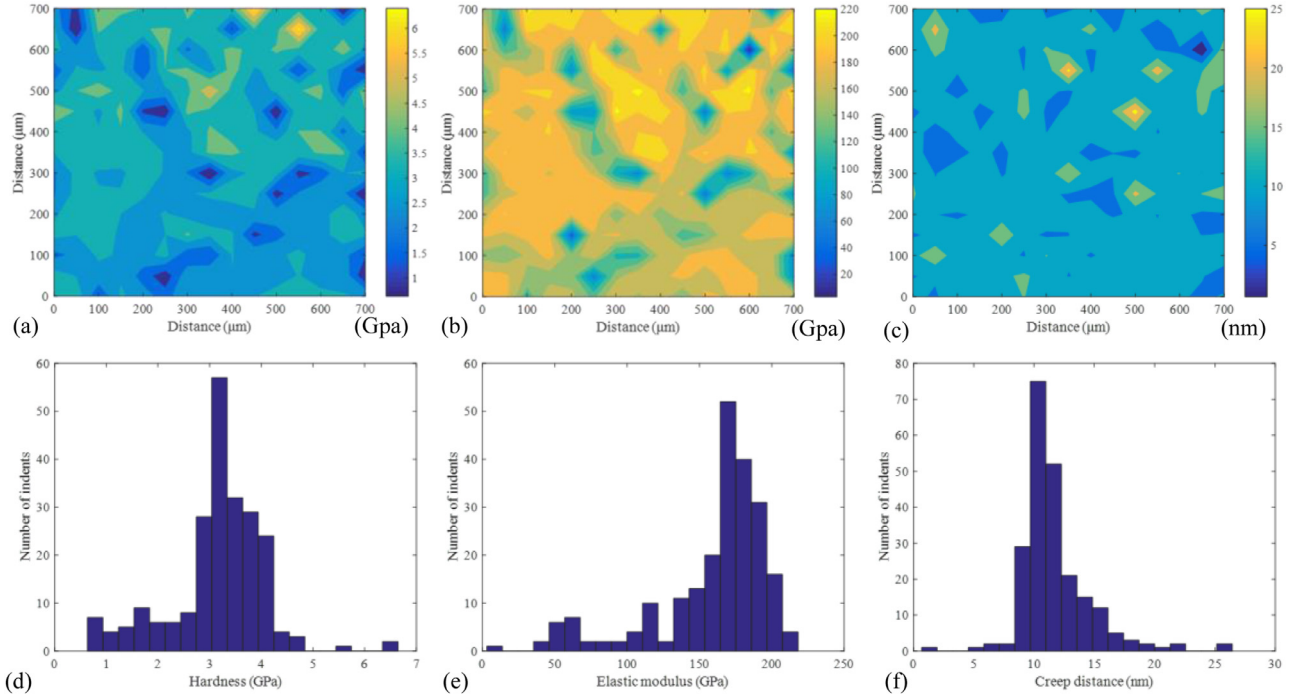

Fig. 4. The distributions of (a), (d) hardness; (b), (e) elastic modulus; (c), (f) creep distance.

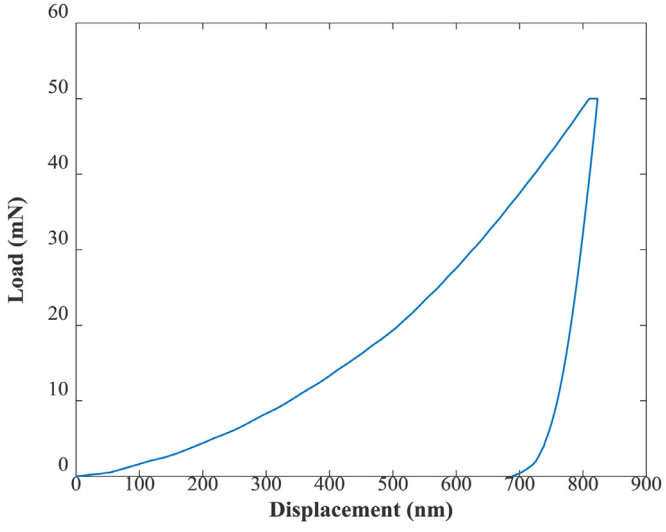

Fig. 5. The statistical result of grid-design nanoindentation.

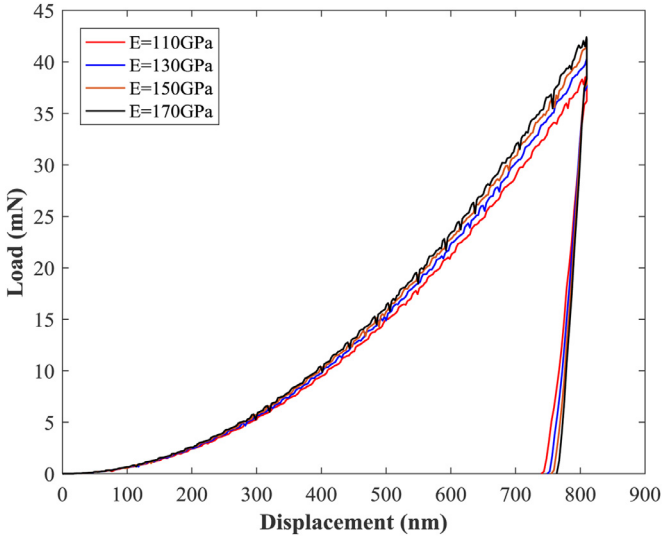

Fig. 6. Load-displacement curves with different *E*.

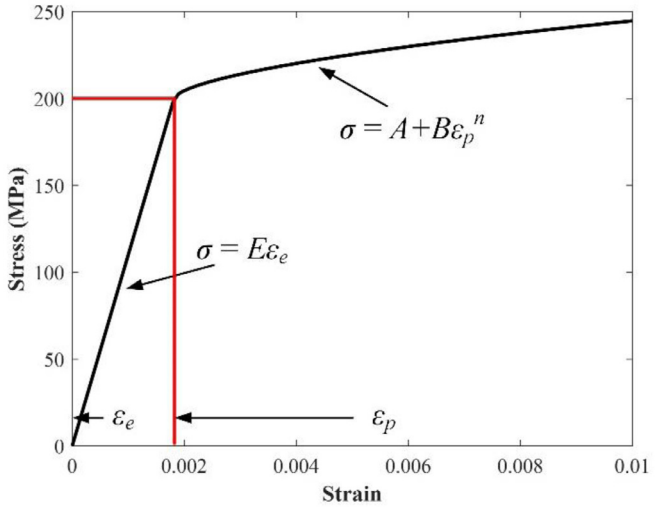

Fig. 7. The common shape of the stress-strain curve.

Poisson's ratio is 0.38. The sensitivity of the simulated results with respect to the value of Young's modulus is also investigated to improve the effectiveness of the proposed method. Fig. 6 illustrates the different loading and unloading curves with various modulus. It can noticed that the simulated results have insignificant difference between each other when the elastic modulus changes from 110 GPa to 170 GPa. This phenomenon represents that the plastic behavior is dominate in sharp indentation. Thus, the priori-estimated E may not result in a large error of the identified stress-strain relation.

The elastic-plastic response of grey cast iron is considered nonlinear with plastic behavior modeled as a power law function, as shown in Fig. 7. The expression of stress-strain relation can be determined as

$$\sigma = \begin{cases} E\varepsilon_e, \text{elastic} \\ A + B\varepsilon_p^{\ n}, \text{plastic} \end{cases} \tag{1}$$

where σ is the stress, ε_e is the elastic strain, ε_p is the plastic strain. A, B, n are the constants of the expression of plastic behavior. The plastic behavior is the same as the first term of Johnson-Cook's law. The strain rate sensitivity and thermal softening are neglected in this section because the deformation in nanoindentation is very slow and there is almost no temperature rise.

The model set in ABAQUS is shown in Fig. 8, simplified as an axisymmetric two-dimensional model. The radius of the tip of the indenter is calibrated by the indentation tests on fuse silicon. The meshing is locally refined to make the simulation more accurate. The process of indentation is given as well with the mapping of stress.

4.2. Three-factor and three-level simulations

As shown in Eq. (1), the stress-strain relation can be modeled as long as the values of A, B, n are achieved. In order to generate a predictable correlation between input constants and the indentation curve, a data set based on finite element simulation needs to be generated. The objective is to minimize the error between predicted and measured loading curves, that is, to find a couple of A, B, n that can provide a loading curve perfectly fitted with that shown in Fig. 5. Moreover, we need to characterize the loading curve with quantifiable value. In this section, the mean error between the prediction and measured curve is set as the objective. More specifically, the mean error is defined by choosing 20 uniform distributed points on the predicted loading curve and calculate the mean error between predicted and measured results. The equation of mean error can be expressed as

$$ME = \frac{\sum_{i=1}^{N} (L_{pi} - L_{mi})}{N} \tag{2}$$

where N is the number of points and is set as 20 in this section. L_{pi} and L_{mi} are the predicted load and measured load of the ith point. The definition of mean error should be distinguished from the conventional Mean Square Error (MSE). This mean error can help to judge the difference between predicted and measured results and determine that the predicted curve is upper or lower than the measured curve.

The simulation set up considering three factors and three levels are shown in Table 1. The output will be the maximum load at the maximum depth. The full-factor and full-level simulations are done to enhance the data set.

The simulated results of all the 27 tests are shown in Table 2. The 27 tests will be used as training set and test set to generate the SVR model in Section 5. Moreover, 6 more simulation with different plastic behavior are done and can be treated as validation set. It can be noticed that the mean error between predicted and measured results ranges from −22.205mN to 18.3893mN, which proves that the levels of A, B, n is enough to capture the measured result that corresponding to 0 mean error.

The mean effects of A, B, n based on 27 full-factor and full-level simulations are illustrated in Fig. 9 to show the sensitivity of the mean error to the constants in stress-strain relation. It can be observed from Figs. 9(a) − 9 (c) that all the three parameters have significant influence on the simulation results. First of all, the predicted results will increase with the growth of A and B, while decrease with the growth of n as shown in Fig. 9. Comparing Figs. 9(a) and 9(b), the trends of mean error with respect to A or B are almost linear. Moreover, the effect of A is

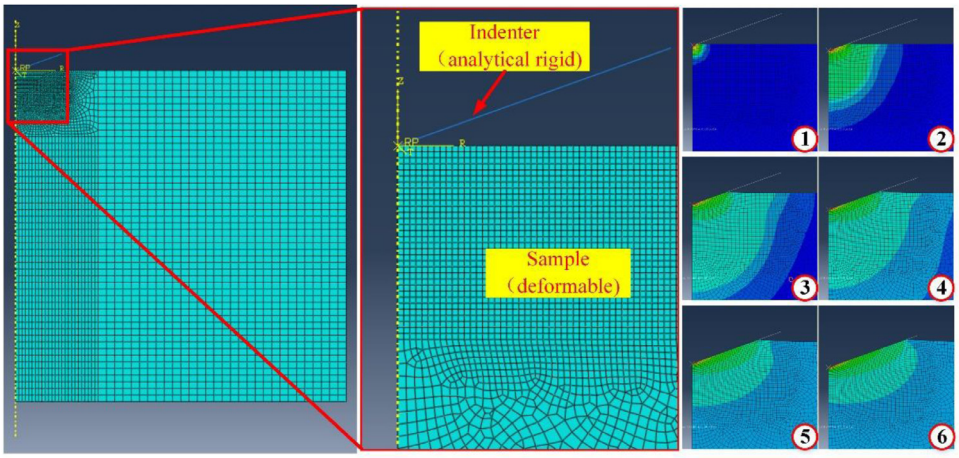

Fig. 8. The model set and the process of indentation in finite element simulation.

Table 1
Three-factor and three-level design.

Factor	*A* (MPa)	*B* (MPa)	*n*
Level 1	100	100	0.01
Level 2	550	550	0.5
Level 3	1000	1000	0.99

Table 2
Predicted results of full-factor and full-level simulations.

Test number	*A* (MPa)	*B* (MPa)	*n*	Mean error (mN)
1	100	100	0.01	−19.4326
2	100	100	0.5	−21.6967
3	100	100	0.99	−22.205
4	550	100	0.01	−6.7272
5	550	100	0.5	−8.558
6	550	100	0.99	−8.901
7	1000	100	0.01	3.4293
8	1000	100	0.5	1.9447
9	1000	100	0.99	1.6931
10	100	550	0.01	−7.0881
11	100	550	0.5	−19.0282
12	100	550	0.99	−21.2843
13	550	550	0.01	2.9975
14	550	550	0.5	−6.2794
15	550	550	0.99	−8.0748
16	1000	550	0.01	11.5726
17	1000	550	0.5	3.7706
18	1000	550	0.99	2.2243
19	100	1000	0.01	2.7648
20	100	1000	0.5	−16.6436
21	100	1000	0.99	−20.5084
22	550	1000	0.01	11.317
23	550	1000	0.5	−4.2118
24	550	1000	0.99	−7.3899
25	1000	1000	0.01	18.3893
26	1000	1000	0.5	5.4637
27	1000	1000	0.99	2.7876
28	300	600	0.2	−6.1517
29	600	900	0.3	2.1396
30	900	300	0.4	1.1974
31	300	900	0.6	−12.743
32	600	300	0.7	−6.7943
33	900	600	0.8	0.4163

more significant than that of *B* due to the larger growth of mean error with *A* and *B* increase from 100 MPa to 1000 MPa. As shown in Fig. 9(c), there is a dramatically drop of the mean error when *n* increase from 0.01 to 0.5. When *n* increase from 0.5 to 0.99, there is a slight reduction in the mean error.

5. SVR-PSO-based inverse method

Although FEM is good at calculating, the simulated results are unpredictable without a mathematical expression. Thus, a surrogate model is required to replace FEM and try to be in accord with the simulated results. What is more, a surrogate model makes the optimization algorithm possible by developing an integrated computer program. This method is better than the conventional finite element support optimization method (Bouzakis et al., 2001; Daphalapurkar et al., 2011), without manual adjustments, and independent of experience. With the development of machine learning theory and computer technology, machine learning based methods are more and more applied to solve the inverse problems in science and engineering. Li et al. (2014) proposed a method integrate with ANN (Artificial Neural Network) and GA (Genetic Algorithm) to obtain the full distribution of stress in rock mass based on the sparse stress measurements. Wang and Adachi (2019) used a machine learning tool to predict the properties of steels. Further, the inverse analysis from properties to microstructure of steels is achieved with satisfactory performance. Jung et al. (2019) correlated the physical variables and material properties using a GPR (Gaussian Process Regression) approach based on the reproduced data set given by simulations of dual phase steels.

In this section, a hybrid method, namely SVR-PSO approach is proposed for inverse exploration of stress-strain relation based on related loading curve of nanoindentation. The surrogate model is a novel method based on machine learning, which has been more and more popular when solving engineering issues. Artificial Neural Networks (ANN) and SVR are two conventional methods to generate a surrogate model to describe the quantitative relation between inputs and outputs in arbitrary dimensions. However, more and more scholars found that the performance of ANN strongly depends on the size of dataset. In this paper, the dataset only contains 27 tests, which may reduce the effectiveness of ANN. SVR is a powerful machine learning tool that can map the input to a high-dimensional feature space to fit the output. Further, SVR is proved to be more suitable to a small database when comparing with ANN (Smola and Schölkopf, 2004). PSO is a commonly used meta-heuristic algorithm without coding and decoding, which makes it easier to conduct. In summary, the machine learning method SVR serves to generate the correlation between parameters of the stress-strain function and mean error based on the data set generated through precise finite element simulations. Then, the meta-heuristic algorithm PSO serves to quick search of the optimal couple of parameters of stress-strain function that fit the measured loading curve most perfectly.

5.1. Modeling based on svr

As a widely used SVR, ε-SVR serves the regression and RBF (Radial Basis Function) is chosen as the kernel function. The parameter *p* in loss function is valued 0.01. This method is supported by the widely used machine learning tool LIBSVM (Chang and Lin, 2011).The input and output used in this section are illustrated in Table 2, which means the input is a three-dimensional data [*A B n*] and the output is the mean

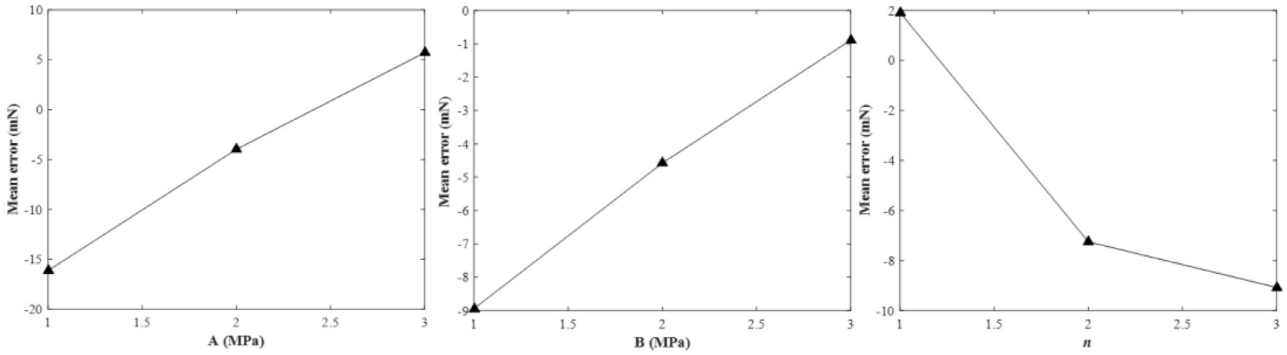

Fig. 9. The mean effects of (a) *A*, (b) *B*, (c) *n* on mean error, respectively.

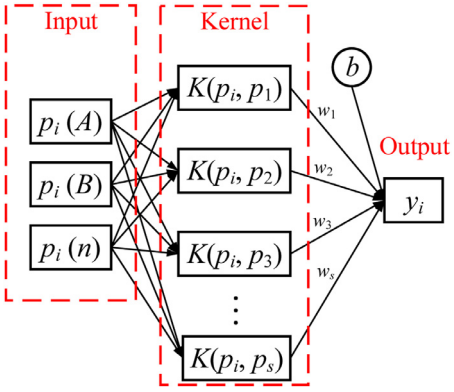

Fig. 10. The model structures of SVR.

error. The model structures of SVR is given in Fig. 10 (Kong et al., 2015). p_i is the ith input data and y_i is the ith output data. In this paper, each input is a three dimensional value, including A, B, n. K is the kernel function, which enables linear regression by transforming the initial input data into higher dimensional feature space (Yoo et al., 2016). s is the number of support vectors, which is not less than the dimension of input and no greater the number of input-output couples. w and b are the weight and bias of support vector, respectively.

Both input and output data should be normalized before the regression to avoid the influence of the difference between data in different dimensions. The expression of normalization can be described as

$$N^* = \frac{N - N_{\min}}{N_{\max} - N_{\min}} \tag{3}$$

where N is the original value of data, N^* is the normalized value of N, $N_{\min}$ and $N_{\max}$ are the minimum and maximum of data, respectively. After the normalization, the ranges of all the features can be unified as [0, 1].

There are two important parameters when using ε-SVR for regression, that is, the penalty coefficient C and the parameter γ of RBF. C means the tolerance for the errors while γ describes the distribution of the values in feature space after mapping. The values of C and γ are determined by grid search in this section, which can accurately achieve the global optimal. Moreover, the simulation data set is divided into nine parts for cross-validation to improve the performance of ε-SVR. The optimal values of C and γ are finally calculated as $C = 2.8284$, $\gamma = 0.7578$. The comparison of the simulated and fitted results are given in Fig. 11.

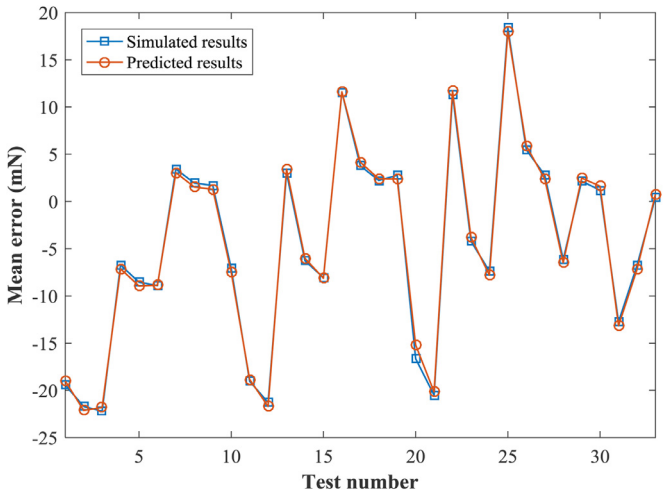

Fig. 11. The comparison of simulated and fitted results with the optimal C and γ.

It can be found in Fig. 11 that ε-SVR can effectively generate a surrogate model to correlate the input (A, B, n) and the output (mean error) for the training set and test set. Moreover, the validation set also shows that the predicted results match the simulated results very well. The perfect performance of SVR can be expected, because the dataset are given by simulation without any error or noise. Different from the experimental methods, finite element method works as a calculator with mathematical model behind. There must be a clear relationship between the input and output. SVR is a powerful tool that can generate the relation in any dimensions, which ensure the accuracy of the predicted results.

5.2. Optimization based on pso

The surrogate model helps to correlate the parameters of stress-strain relation and the mean error. An optimization algorithm is required to find the optimal parameters to perfectly match the predicted result with that given by nanoindentation. As a meta-heuristic algorithm, PSO is widely used in lots of literature for its ability of quick search (Weng et al., 2020). It can obtain the optimal solution based on a group of particles. Each particle has two characteristics, that is, the position and velocity. The position characterizes the current solution while the velocity characterizes the search direction considering both the global best solution and individual best solution. These two characteristics update in each generation and the function can be expressed as

$$\begin{cases} v_{i,j+1} = \eta v_{i,j} + c_1 r_1 (P_{i,best} - p_{i,j}) + c_2 r_2 (G_{best} - p_{i,j}) \\ p_{i,j+1} = p_{i,j} + v_{i,j+1} \end{cases} \tag{4}$$

where $p_{i,j}$ and $v_{i,j}$ represent the position and velocity of the jth generation of ith particle while $p_{i,j+1}$ and $v_{i,j+1}$ represent the position and velocity of $(j+1)$th generation of ith particle. c_1 and c_2 are the cognitive parameter and the social parameter, respectively. r_1 and r_2 are random factors within [0, 1]. $P_{i,best}$ is the individual best solution of ith particle and G_{best} is the global best solution. η is the inertia factor, which can keep the global search ability of particles in the early generations and enhance the local search ability in the later generations. Table 3 describes the parameters of PSO used in this section.

Fig. 12 illustrates the evolution of the global fitness during the optimization. It can be found that this algorithm works very well to find the optimal solution, achieving the optimum within 27 generations. The global fitness, namely the mean error is extremely small after the optimization. The final solution is also given in Fig. 12, with $A = 836$ MPa, $B = 711$ MPa, $n = 0.6421$.

The stress-strain curve with the best solution taken into account is shown in Fig. 13. The yield stress is 836 MPa, the elastic behavior and plastic behavior are significantly different from each other. The stress can hardly increase with the growth of plastic strain.

To validate the correctness of the inverse method, one more simulation is done using the optimal couple of A, B, n and the comparison of the predicted and measured loading curves are given in Fig. 14. The predicted loading curve fits pretty well with the measured one, especially at the later period, which proves the effectiveness of the method proposed in this paper.

Table 3
The parameters of PSO.

Parameter	Value
Population size	100
The range of particle velocity	[−1,1]
The range of particle position	[100 100 0.01]-[1000 1000 0.99]
Inertia weight (η)	0.9–0.3 (linearly)
c_1, c_2	1.49, 1.49
The maximum number of iterations	100

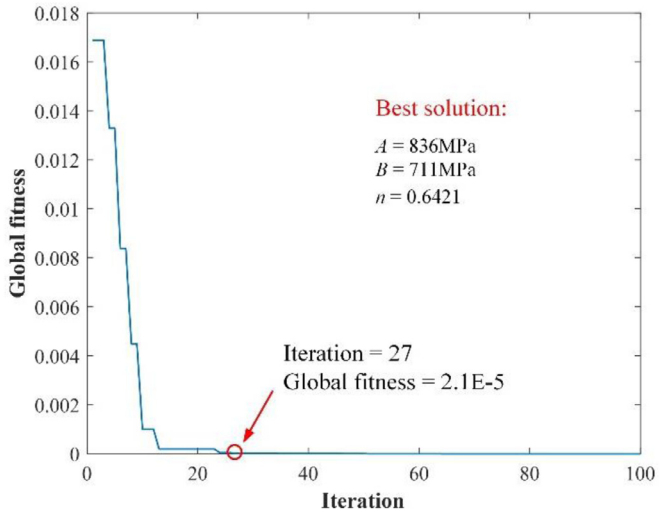

Fig. 12. The evolution of the global fitness.

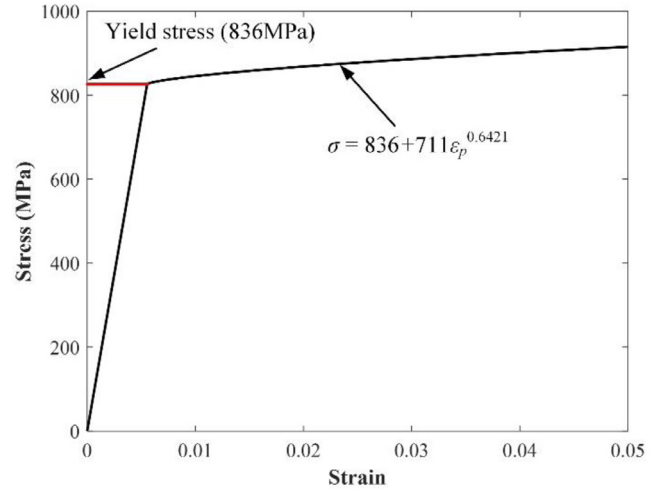

Fig. 13. The calibrated stress-strain curve of grey cast iron.

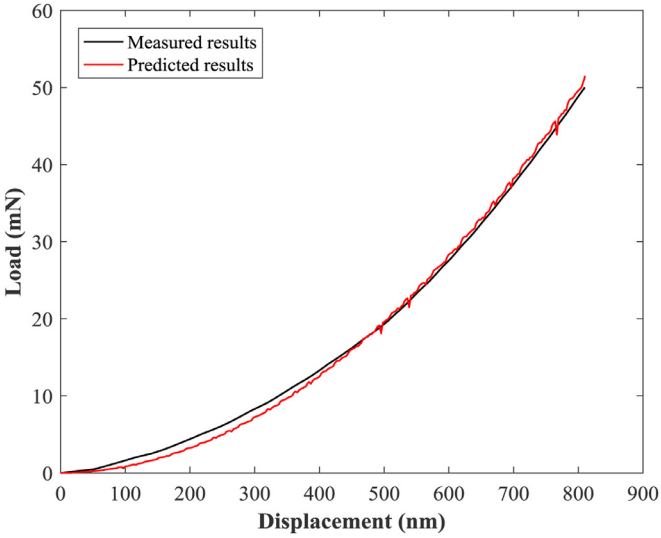

Fig. 14. The fitting results using the optimal stress-strain curve.

6. Conclusions

Recently, extracting the stress-strain relationship from instrumented nanoindentation achieves more and more attention of the scholars and companies. This paper presents an intelligent and effective method to model the stress-strain curve from sharp indentation data for grey cast iron. FEM, machine learning tool, and optimization algorithm support to solve this problem. The comparison between predicted and measured results shows the correctness of the inverse method. The contributions are drawn below.

(1) Grid nanoindentation is performed on grey cast iron to achieve the statistical results of heterogeneous material. The mapping of hardness and modulus are given to show the distributions of mechanical properties of the material. The average loading and unloading curve is calculated to represent the macro material response.
(2) A precise finite element model is established for indentation simulation with a power law constitutive model. The constants of stress-strain function are considered to design the three-factor and three-level simulations. The simulation data set is generated using the full-factor and full-level design.
(3) SVR serves to correlate the constants in stress-strain relation and the maximum load based on the FEM data set. The best parameters of support vector machine are determined by cross-validation and grid search. The surrogate model shows very good performance when comparing the results provided by FEM and SVR.
(4) PSO is chosen as the optimization algorithm to find the optimal solution to fit the measured results based on the surrogate model given by SVR. This algorithm is modified with an inertia factor to improve the local search ability of the algorithm. The optimal values of the constants in stress-strain function is applied for the simulation and the predicted loading curve perfectly fit with the measured curve, which validates the effectiveness and correctness of the inverse method proposed in this paper.

Declaration of Competing Interest

The authors declare that they have no known competing financial interests or personal relationships that could have appeared to influence the work reported in this paper.

Acknowledgments

This work is partially supported by the National Natural Science Foundation of China (51705385, 51975237, and 51805380), China Scholarship Council (201906950051), and The Fundamental Research Funds for the Central Universities (2019-YB-019).

References

Bouzakis, K.-.D., Michailidis, N., Erkens, G., 2001. Thin hard coatings stress–strain curve determination through a FEM supported evaluation of nanoindentation test results. Surf. Coat. Tech. 142, 102–109.
Chang, C.-.C., Lin, C.-.J., 2011. LIBSVM: a library for support vector machines. ACM T. Intel. Syst. Tec. 2, 27.
Chen, L., Ståhl, J.E., Zhou, J., 2015. Analysis of in situ mechanical properties of phases in high-alloyed white iron measured by grid nanoindentation. J. Mater. Eng. Perform. 24, 4022–4031.
Collin, J.-.M., Mauvoisin, G., El Abdi, R., 2008. An experimental method to determine the contact radius changes during a spherical instrumented indentation. Mech. Mater. 40, 401–406.
Dao, M., Chollacoop, N.v., Van Vliet, K., Venkatesh, T., Suresh, S., 2001. Computational modeling of the forward and reverse problems in instrumented sharp indentation. Acta. Mater. 49, 3899–3918.
Daphalapurkar, N., Wang, F., Fu, B., Lu, H., Komanduri, R., 2011. Determination of mechanical properties of sand grains by nanoindentation. Exp. Mech. 51, 719–728.
Dean, J., Aldrich-Smith, G., Clyne, T., 2011. Use of nanoindentation to measure residual stresses in surface layers. Acta. Mater. 59, 2749–2761.
Donohue, B.R., Ambrus, A., Kalidindi, S.R., 2012. Critical evaluation of the indentation data analyses methods for the extraction of isotropic uniaxial mechanical properties

using finite element models. Acta. Mater. 60, 3943–3952.
Fischer-Cripps, A.C., 2006. Critical review of analysis and interpretation of nanoindentation test data. Surf. Coat. Tech. 200, 4153–4165.
Giannakopoulos, A., Suresh, S., 1999. Determination of elastoplastic properties by instrumented sharp indentation. Scripta. Mater. 40, 1191–1198.
Golovin, Y.I., 2008. Nanoindentation and mechanical properties of solids in submicrovolumes, thin near-surface layers, and films: a Review. Phys. Solid. State + 50, 2205–2236.
Hamim, S.U., Singh, R.P., 2017. Taguchi-based design of experiments in training POD-RBF surrogate model for inverse material modelling using nanoindentation. Inverse. Probl. Sci. En. 25, 363–381.
Jung, J., Yoon, J.I., Park, H.K., Kim, J.Y., Kim, H.S., 2019. Bayesian approach in predicting mechanical properties of materials: application to dual phase steels. Mat. Sci. Eng. A-Struct. 743, 382–390.
Kalidindi, S.R., Pathak, S., 2008. Determination of the effective zero-point and the extraction of spherical nanoindentation stress–strain curves. Acta. Mater. 56, 3523–3532.
Kong, X., Liu, X., Shi, R., Lee, K.Y., 2015. Wind speed prediction using reduced support vector machines with feature selection. Neurocomputing 169, 449–456.
Kucharski, S., Mróz, Z., 2007. Identification of yield stress and plastic hardening parameters from a spherical indentation test. Int. J. Mech. Sci. 49, 1238–1250.
Li, F., Wang, J.-a., Brigham, J.C., 2014. Inverse calculation of insitu stress in rock mass using the surrogate-model accelerated random search algorithm. Comput. Geotech. 61, 24–32.
Long, X., Wang, S., Feng, Y., Yao, Y., Keer, L.M., 2017. Annealing effect on residual stress of Sn-3.0 Ag-0.5 Cu solder measured by nanoindentation and constitutive experiments. Mat. Sci. Eng. A-Struct. 696, 90–95.
Ma, Z., Long, S., Zhou, Y., Pan, Y., 2008. Indentation scale dependence of tip-in creep behavior in Ni thin films. Scripta. Mater. 59, 195–198.
Ma, Z., Zhou, Y., Long, S., Lu, C., 2012a. On the intrinsic hardness of a metallic film/substrate system: indentation size and substrate effects. Int. J. Plasticity 34, 1–11.
Ma, Z., Zhou, Y., Long, S., Zhong, X., Lu, C., 2012b. Characterization of stress-strain relationships of elastoplastic materials: an improved method with conical and pyramidal indenters. Mech. Mater. 54, 113–123.
Moy, C.K., Bocciarelli, M., Ringer, S.P., Ranzi, G., 2011. Identification of the material properties of Al 2024 alloy by means of inverse analysis and indentation tests. Mat. Sci. Eng. A-Struct. 529, 119–130.
Oliver, W.C., Pharr, G.M., 2004. Measurement of hardness and elastic modulus by instrumented indentation: advances in understanding and refinements to methodology. J. Mater. Res. 19, 3–20.
Patel, D.K., Kalidindi, S.R., 2016. Correlation of spherical nanoindentation stress-strain curves to simple compression stress-strain curves for elastic-plastic isotropic materials using finite element models. Acta. Mater. 112, 295–302.
Pathak, S., Kalidindi, S.R., 2015. Spherical nanoindentation stress–strain curves. Mat. Sci. Eng. R 91, 1–36.
Pathak, S., Shaffer, J., Kalidindi, S.R., 2009. Determination of an effective zero-point and extraction of indentation stress–strain curves without the continuous stiffness measurement signal. Scripta. Mater. 60, 439–442.
Ripley, M.I., Kirstein, O., 2006. Residual stresses in a cast iron automotive brake disc rotor. Physica B 385, 604–606.
Schwarm, S.C., Kolli, R.P., Aydogan, E., Mburu, S., Ankem, S., 2017. Characterization of phase properties and deformation in ferritic-austenitic duplex stainless steels by nanoindentation and finite element method. Mat. Sci. Eng. A-Struct. 680, 359–367.
Smola, A.J., Schölkopf, B., 2004. A tutorial on support vector regression. Stat. Comput. 14, 199–222.
Tabor, D., 2000. The Hardness of Metals. Oxford university press.
Wang, Z.-.L., Adachi, Y., 2019. Property prediction and properties-to-microstructure inverse analysis of steels by a machine-learning approach. Mat. Sci. Eng. A-Struct. 744, 661–670.
Weaver, J.S., Kalidindi, S.R., 2016. Mechanical characterization of Ti-6Al-4V titanium alloy at multiple length scales using spherical indentation stress-strain measurements. Mater. Design. 111, 463–472.
Weng, J., Zhuang, K., Hu, C., Ding, H., 2020. A PSO-based semi-analytical force prediction model for chamfered carbide tools considering different material flow state caused by edge geometry. Int. J. Mech. Sci. 169, 105329.
Yoo, K.H., Back, J.H., Na, M.G., Kim, J.H., Hur, S., Kim, C.H., 2016. Prediction of golden time using SVR for recovering SIS under severe accidents. Ann. Nucl. Energy. 94, 102–108.
Zhang, Q., Li, X., Yang, Q., 2018. Extracting the isotropic uniaxial stress-strain relationship of hyperelastic soft materials based on new nonlinear indentation strain and stress measure. AIP Adv. 8, 115013.